Structure of End-Grafted Polymer Brushes in Liquid and Supercritical Carbon Dioxide: A Neutron Reflectivity Study

Stephen M. Sirard,[§] Ravi R. Gupta,[†] Thomas P. Russell,[‡] James J. Watkins,[†] Peter F. Green,[§] and Keith P. Johnston*,[§]

Department of Chemical Engineering, University of Texas at Austin, Austin, Texas 78712; Department of Chemical Engineering, University of Massachusetts, Amherst, Massachusetts 01003; and Department of Polymer Science and Engineering, University of Massachusetts, Amherst, Massachusetts 01003

Received November 4, 2002; Revised Manuscript Received February 25, 2003

ABSTRACT: Neutron reflectivity was used to characterize the structure of end-grafted deuterated poly(dimethylsiloxane) (*d*-PDMS) brushes on SiO_x wafers exposed to liquid and supercritical carbon dioxide (CO_2). The solvent quality was tuned continuously over a large range from ideal gas conditions to a near-Θ solvent by varying temperature and CO_2 density. Two distinct regions were seen in the segment density profile as a function of distance from the surface: (i) an inner concentrated region near the substrate where the segment density is high due to the strong attractive short- and long-ranged interactions between the *d*-PDMS and the SiO_x substrate and the attractive intra- and interchain interactions and (ii) an outer solvated region that is dilute in polymer due to solvation by CO_2. In the outer solvated region, the well-defined block profile at the worst solvent conditions changes to a more parabolic profile with improving solvent quality. The thickness and volume fraction profiles for the outer solvated region change much more with solvent quality than has been seen in previous studies with incompressible solvents, due to the high asymmetry in the intermolecular interactions as well as the large compressibility and free volume differences between the polymer segments and the solvent.

Introduction

Liquid and supercritical carbon dioxide (CO_2) have emerged as alternatives to toxic organic solvents.[1] Not only is CO_2 essentially nontoxic, but it is abundant, inexpensive, and nonflammable. Furthermore, the critical temperature of CO_2, 31.1 °C, is not far from room temperature, and its solvent quality can be tuned markedly with small variations in pressure and temperature. The tunable solvation properties of CO_2 offer many potential advantages in the synthesis, processing, and separation of colloidal dispersions, such as water-in-CO_2 emulsions and microemulsions,[2,3] polymer latexes,[4] and dispersions of inorganic metals and metal oxides.[5] Since CO_2 has no dipole moment and has a low polarizability per volume (i.e., weak van der Waals interactions), many nonvolatile compounds are insoluble in CO_2. A significant challenge in the design of CO_2-based stabilizers is to provide sufficient solvation by CO_2 such that steric repulsive forces overcome attractive van der Waals forces between surfaces. It has been found that polymers with low surface tension, and hence low cohesive energy density, are most effective as CO_2 stabilizers. "CO_2-philic" stabilizers include fluoroacrylates, fluoroethers, siloxanes, poly(propylene oxide)s, polycarbonate copolymers, acetylated sugars, and some hydrocarbons.[6−12] McClain et al.[13] showed with small-angle neutron scattering (SANS) that poly(1,1-dihydroperfluorooctyl acrylate) (PFOA) has a positive second virial coefficient (A_2) in CO_2 at 65 °C and 340 bar, whereas Chillura-Martino et al.[14] found a negative A_2 for PDMS at the same conditions. However, Melnichenko et al.[15] showed that CO_2 is a good solvent for PDMS at higher CO_2 densities.

One of the most clearly defined methods for stabilizing dispersions is to terminally attach polymers onto the surfaces of the particles.[16] Surfaces containing dense end-grafted polymers will repel each other in a sufficiently good solvent when the stabilizing layers are thick enough to screen the attractive van der Waals forces between the particle cores. If the monomer density becomes sufficiently large in an end-grafted polymer layer, the polymer chains will stretch away from the surface and form a polymer brush. Chains immersed in a good solvent will have the tendency to maximize energetically favorable contacts with the solvent molecules and avoid contacts with neighboring chains. Therefore, the equilibrium brush structure and height will be determined by a balance between the interactions that promote stretching and the associated loss of chain conformational entropy.[17]

The structures of polymer brushes exposed to incompressible liquid solvents have been investigated with scaling analysis,[18] self-consistent field theory (SCF),[19,20] simulation,[21,22] and experiment.[23−25] There is a general consensus that the concentration profile is parabolic for a brush on a noninteracting surface in a good solvent. When the chains are grafted to a repulsive or noninteracting surface, there exists a depletion of segments near the grafting surface. Simulation and experimental studies often show an exponential decay in the concentration profile near the brush/solvent interface.

There has been recent progress in probing polymer brushes in solvents with techniques such as ellipsometry,[26] SANS,[27] and neutron reflectivity.[23−25,28,29] Neutron reflectivity (NR) is a particularly useful technique for probing polymer brushes because it is nondestruc-

[†] Department of Chemical Engineering, University of Massachusetts.
[‡] Department of Polymer Science and Engineering, University of Massachusetts.
[§] Department of Chemical Engineering, University of Texas at Austin.
* Corresponding author. E-mail: kpj@che.utexas.edu.

10.1021/ma025801w CCC: $25.00
Published on Web 04/03/2003

tive, with a depth resolution of ~1 nm.[30,31] Furthermore, contrast can be manipulated easily by using isotopic labeling.[30,31] In general, experimentally determined brush structures in conventional liquid solvents have shown good agreement with predictions from theory[19,20] and simulations.[21,22] For example, NR results by Karim et al. for the swelling and density profiles of end-grafted polystyrene brushes in cyclohexane and toluene at various solvent qualities were in good agreement with SCF predictions.[23]

While advances have been made in understanding brushes exposed to incompressible solvents, few studies have investigated the behavior of polymer brushes in supercritical solvents, where the solvent quality is a strong function of solvent density. Peck and Johnston[32] combined SCF theory with lattice fluid theory (LFSCF), to include effects of compressibility, to model the structure and interactions between short terminally attached chains in a supercritical solvent. Meredith and Johnston[33] used LFSCF to examine the structure of high molecular weight adsorbed copolymers and end-grafted stabilizers as a function of solvent quality in a supercritical fluid. They concluded that as the solvent density is lowered, adsorbed and end-grafted chains collapse as the solvent gains entropy by expanding away from the chains and into bulk solution. Furthermore, they predicted that flocculation of two coated surfaces occurs at the upper critical solution density (UCSD) of the stabilizer in bulk solvent. The results were corroborated by Monte Carlo simulations for the structure and interactions of end-grafted chains in a compressible solvent[34] as well as in stability studies of poly(2-ethylhexyl acrylate) emulsions in supercritical CO_2.[35] Other experimental studies on stabilizer structure in supercritical fluids have focused on the formation and structure of block copolymer and surfactant micelles.[3,36−38] Measurements of the interfacial structure of chemically end-grafted brushes in supercritical solvents have not been reported previously, despite their importance in numerous applications.

The primary objective of this work is to tune the solvent quality of a supercritical fluid with temperature and pressure to manipulate the chain extension and segment density profile of an end-grafted homopolymer brush. Deuterated poly(dimethylsiloxane) (*d*-PDMS) was end-grafted onto silicon wafers to form dense brushes. In-situ neutron reflectivity experiments were used to measure the thickness and volume fraction profiles of the brushes as a function of temperature and CO_2 density (or solvent quality). The range in solvent quality is enormous from nonsolvent conditions to a near-Θ solvent, as the density of CO_2 ranges from ~0 to 0.92 g/cm^3. As a function of solvent quality, we demonstrate that hydrogen bonding and Hamaker forces between the substrate and chains along with attractive intra- and interchain interactions that act to collapse the chains compete with the solvation forces that act to stretch the chains, leading to two distinct regimes in the brush concentration profile. The major differences in the brush profiles relative to those in incompressible solvents are explained in terms of the large asymmetry in the intermolecular forces, the compressibility of the solvent, and the long-range Hamaker forces between the surface and chains. The results are compared with previous theory[32,33] and simulation[34] of brushes in compressible solvents with emphasis on the brush structure at densities near the

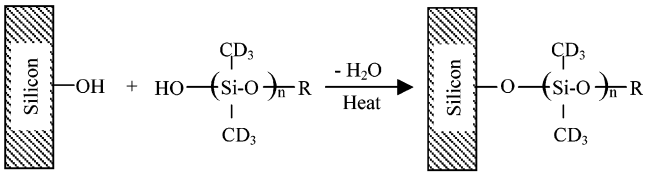

Figure 1. Grafting reaction. R = Si(CD$_3$)$_3$.

previously determined UCSD[39] and Θ density[15,40] (ρ_Θ) for the free polymer in solution.

Experimental Section

Materials. *d*-PDMS (M_w = 16 000, M_w/M_n = 1.28) with a monofunctional silanol end group was purchased from Polymer Source. The *d*-PDMS films were spin-coated onto silicon (100) wafers (Wafer World) from heptane solutions.

Sample Preparation. The wafers were cut into 2 in. × 2 in. squares and were initially cleaned[41] by soaking in a 50:50 (w/w) hydrochloric acid/methanol (EM Science) solution for 30 min. The wafers were then rinsed with excess deionized water (NANOpure II, Barnstead) and dried with nitrogen gas (Air Products, >99.9999%). The wafers were then soaked in 95% sulfuric acid (Mallinckrodt, analytical grade) for 30 min and subsequently rinsed with deionized water and dried with nitrogen gas.

Prior to coating the *d*-PDMS, the native oxides on the silicon wafers were characterized with a spectroscopic ellipsometer (J.A. Woollam). The native oxide was between 1.2 and 1.5 nm thick for all of the samples. Thick *d*-PDMS films were spun onto the wafers using a photoresist spinner (Headway Research, Inc.). The concentration of the *d*-PDMS/heptane solution and the spinning speed were adjusted to control the film thickness. The coated wafers were annealed under vacuum at 125 °C for 5 days to graft the *d*-PDMS according to the reaction shown in Figure 1. After annealing, the *d*-PDMS-coated wafers were rinsed with excess amounts of pure heptane to remove any nonattached polymer. The thickness of the end-grafted *d*-PDMS brushes was measured with the ellipsometer (assuming $n_{d-\mathrm{PDMS}}$ = 1.42). To ensure that all the *d*-PDMS chains were attached to the substrate, samples were soaked in heptane for an additional 2 h, dried with nitrogen gas, and placed under vacuum overnight at room temperature. No significant change in the brush thickness was seen after this additional soaking.

Neutron Reflectivity. The NR experiments were performed on the SURF time-of-flight reflectometer at ISIS-Rutherford Appleton Laboratory, UK. The experiments were performed in a stainless steel high-pressure NR cell that has been described elsewhere.[42,43] The cell was heated with cartridge heaters, and CO_2 was charged to the cell using a computer-controlled syringe pump (ISCO Products Inc.).

The principles of NR have been detailed elsewhere.[30] The NR profiles were obtained as a function of the neutron momentum transfer normal to the substrate:

$$k = \left(\frac{2\pi}{\lambda}\right)\sin(\theta) \qquad (1)$$

where λ is the neutron wavelength and θ is the grazing angle of incident. k was varied between 0.004 and 0.087 Å^{-1} for all the experiments. The experiments were performed at temperatures of 25 and 65 °C and at CO_2 fluid pressures up to 200 atm. Figure 2 shows the state of the pure CO_2 with respect to the pressure/temperature regimes used in this study. For each temperature, NR profiles were initially collected at atmospheric pressure and then in ascending pressure steps. The time for collecting the NR profiles was between 40 and 70 min at each pressure. After each pressure change, NR profiles were collected after waiting approximately 15 min. The modification of the neutron spectrum due to the presence of high-pressure windows and the CO_2 was taken into account when calculating the reflectivity. Spectroscopic ellipsometry measurements on

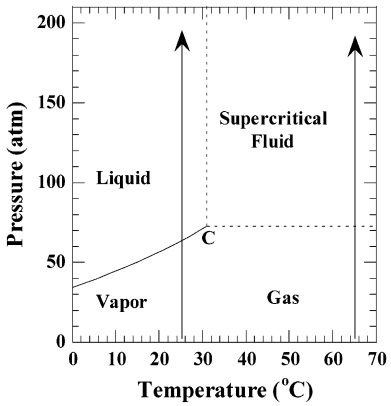

Figure 2. Pressure−temperature phase diagram for pure CO_2. (—) is the liquid−vapor saturation curve, and the (↑) represent the pressure/temperature paths used in this study.

the *d*-PDMS brush showed that the thickness of the brush, after exposure to the same CO_2 pressures and temperatures as in the NR experiments, was the same within experimental error to the initial brush thickness. This result suggests that the chain extension is reversible and not trapped in a metastable state.

NR is sensitive to variations in the neutron scattering length densities (NSLD) normal to the substrate. To fit the data, a multilayered model was constructed consisting of silicon substrate, native oxide (SiO_x), and *d*-PDMS brush layers as well as a CO_2 atmosphere. The pure component NSLD for each layer was calculated from the following equation[30]

$$\mathrm{NSLD}_i = \frac{b}{v} = \frac{b_i \rho_i N_{\mathrm{Av}}}{M_{\mathrm{w}i}} \tag{2}$$

where b_i is the sum of the neutron scattering lengths of the atoms comprising component i, ρ_i is the mass density of component i, N_{Av} is Avogadro's number, and $M_{\mathrm{w}i}$ is the molecular weight of component i. Literature values were used for the b_i's.[44] The *d*-PDMS brush was broken down into two regions consisting of an inner polymer-concentrated region near the substrate and an outer solvated region. The polymer volume fraction for the concentrated region was assumed to be constant as a function of distance from the grafting plane and was modeled using a step function. The outer solvated region was discretized into 100 layers of equal thickness in which the polymer volume fraction varied with distance, z, from the grafting plane. Thus, the complete model for the PDMS brush is

$$\phi(z) = \phi_{\mathrm{CR}} \qquad 0 \le z \le h_{\mathrm{CR}} \tag{3a}$$

$$\phi(z) = \phi_0\left(1 - \left(\frac{z - h_{\mathrm{CR}}}{h}\right)^2\right)^{\alpha} \qquad h_{\mathrm{CR}} < z \le h_{\mathrm{t}} \tag{3b}$$

where ϕ_{CR} is the polymer volume fraction in the inner concentrated region, h_{CR} is the thickness of the inner concentrated region, ϕ_0 is the polymer volume fraction at the interface between the concentrated region and the solvated region, h is the thickness of the outer solvated region of the brush, and h_{t} is the total thickness of the brush. The thicknesses of the concentrated and solvated regions were summed to get the total brush thickness at each condition.

The profiles were fit using a multilayer recursion method to calculate the total reflectance and reflectivity for the model as described in detail elsewhere.[30] The main fit parameters are the ϕ_0, h, and α in eq 3 for the solvated region, the h_{CR} and NSLD of the polymer-concentrated region, the interfacial roughness (described using an error function representation[30]), and $\Delta k/k$. The best fit to each reflectivity profile was determined by varying the fit parameters in order to minimize the χ^2 error function.

Table 1. Characterization Parameters for *d*-PDMS Brushes

characterization parameters	25 °C	65 °C
h_0 (nm)	10.5	9.4
Γ (mg/m^2)	10.0	9.2
D (nm)	1.63	1.70
σ (chains/nm^2)	0.376	0.346
$\sigma^* = \sigma\pi R_g^2$	13.7	12.6
$\Omega = (a/D)^2$	9.41×10^{-2}	8.65×10^{-2}
h_0/D	6.44	5.53
h_0/R_g	3.09	2.76

Results

Brush Characterization at Ambient Pressure. The initial dry thickness of the brushes without CO_2 was determined with both NR and spectroscopic ellipsometry. NR gave a dry thickness of 10.5 nm for the brush used in the 25 °C experiment and 9.4 nm for the brush used in the 65 °C experiment. Ellipsometry gave a dry thickness of 10.4 and 9.6 nm for the brushes used in the 25 and 65 °C experiments, respectively.

The end-grafted polymers were characterized with several parameters as given in Table 1. For *d*-PDMS, the mass of polymer per unit area, Γ, can be calculated using eq 4

$$\Gamma\ [\mathrm{mg/m^2}] = 0.1\gamma\ [\text{Å}]\rho_{d-\mathrm{PDMS}}\ [\mathrm{g/cm^3}] \tag{4}$$

where $\rho_{d-\mathrm{PDMS}}$ is the density of pure *d*-PDMS and γ is defined as

$$\gamma = \int_0^{h_{\mathrm{t}}} \phi(z)\, \mathrm{d}z \tag{5}$$

The distance between grafting points, D (in Å), is

$$D = \left(\frac{6.023\Gamma}{M_{\mathrm{w}}}\right)^{-1/2} \tag{6}$$

Furthermore, the graft density, Ω, and the overlap concentration, σ^*, can be calculated as follows:

$$\Omega = \left(\frac{a}{D}\right)^2 \tag{7}$$

$$\sigma^* = \sigma\pi R_g^2 \tag{8}$$

where a is the size of a *d*-PDMS monomer (∼5 Å),[45] σ is the number of chains per unit area, and R_g is the unperturbed radius of gyration for *d*-PDMS (∼3.4 nm).[15] The end-grafted *d*-PDMS in this study is clearly in the brush regime, i.e., $\sigma^* \gg 1$, due to excluded-volume interactions. Further evidence of the brush regime is given by the large values of h_0/D and h_0/R_g, where h_0 is the dry thickness of the brush.

Neutron Reflectivity in CO_2. The experimental NR profiles for the *d*-PDMS brushes exposed to CO_2 at different pressures are shown in Figure 3. Qualitatively, it is evident from the reduction in the separation distance of successive minima that the effective thickness of the PDMS at the surface is increasing, which means that the *d*-PDMS chains are extending into the CO_2 as the pressure is increased. The NSLD profiles corresponding to the best fits of the NR profiles are shown in Figure 4. Initially, the polymer volume fraction profiles of the *d*-PDMS brushes were modeled as a function of distance from the grafting plane by eq 3b,

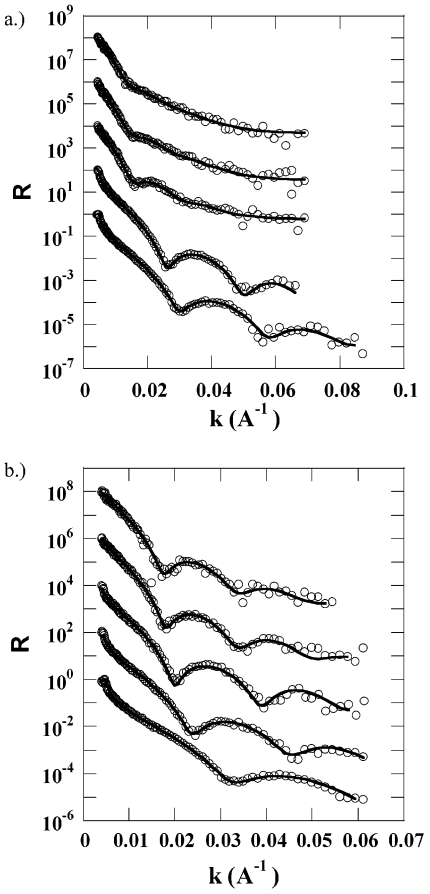

Figure 3. (a) Neutron reflectivity profiles for *d*-PDMS in CO_2 at 25 °C. For clarity, the profiles are offset by various orders of magnitude. Starting from the bottom and moving upward, the profiles correspond to CO_2 pressures of 1.0, 35.2, 123.7, 164.0, and 197.7 atm. (○) are experimental profiles and (—) are best-fit profiles. (b) Neutron reflectivity profiles at 65 °C. Starting from the bottom and moving upward, the profiles correspond to CO_2 pressures of 1.0, 70.5, 96.3, 137.1, and 191.5 atm.

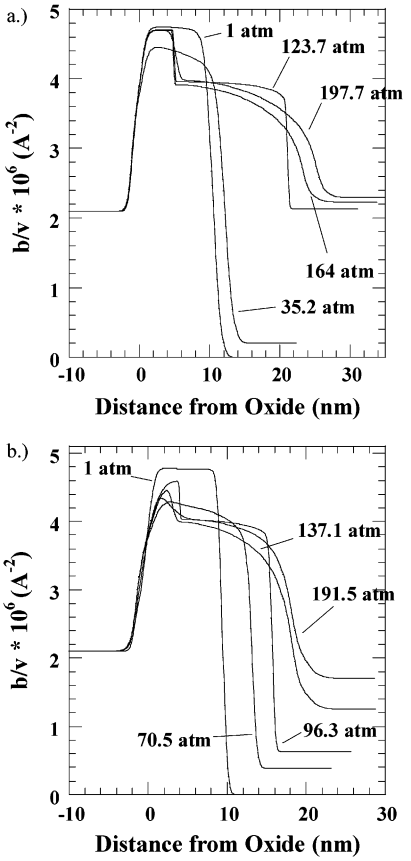

Figure 4. (a) NSLD profiles for *d*-PDMS in CO_2 at 25 °C. (b) NSLD profiles at 65 °C.

where ϕ_0 was the volume fraction of *d*-PDMS at the grafting plane ($z = 0$) and h was the thickness of the brush. The use of this model is motivated by previous experiments[23] and SCF calculations.[19,20] For infinitely long chains, SCF calculations predict that $\alpha = 1$ for a good solvent and $\alpha = {}^1/_2$ for a Θ solvent.[19,20,23] Equation 3b alone, however, did not give sufficiently good fits to the data at higher CO_2 pressures.

The above observation is not surprising as it is well-known that PDMS adsorbs strongly to SiO_x surfaces.[46−50] Furthermore, CO_2 is worse than a Θ solvent at the pressures studied.[15] Interactions between monomer segments of PDMS are stronger than those between a monomer and CO_2. On the basis of each of these factors, one would expect a larger PDMS segmental density near the substrate. Good fits were achieved at all of the conditions with the inclusion of a polymer-concentrated layer in the model (eq 3a). Figure 5 shows reflectivity profiles generated using three different NSLD profiles with an equivalent brush thickness at 65 °C and 137 atm along with the experimental data at this condition. The profile with the polymer-concentrated region (solid line) gives a superior fit to the experimental data over the entire k range relative to the other profiles.

Chain Extension. The total thickness of the *d*-PDMS brushes as a function of CO_2 pressure at both 25 and 65 °C is shown in Figure 6. The total brush thickness is determined by summing the thicknesses of the concentrated and solvated regions, which are determined from the detailed theoretical fit to the reflectivity profiles. The *d*-PDMS chains extend over 100% from their initial thickness at both temperatures. Increasing CO_2 pressure leads to higher CO_2 densities, better solvent qualities, and thus greater extension.

The chain extension at 25 °C is greater than at 65 °C as shown in Figure 6. At a given pressure, the density of CO_2 at 25 °C is markedly higher than at 65 °C, resulting in better solvent quality. However, if the chain extension is plotted vs solvent density as in Figure 7, a different trend is observed. These data indicate that at a given CO_2 density the *relative* chain extension at 65 °C is higher than at 25 °C.

Figure 7 also shows the UCSD for the CO_2/PDMS (M_n = 10 000 g/mol) system at 25 °C (0.908 g/mL) and 65 °C (0.793 g/mL)[39] as well as ρ_Θ (i.e., the UCSD for infinite molecular weight) at 50 °C (0.972 g/mL) and 65 °C (0.950 g/mL).[15,40] In Figures 6 and 7, we see that the chains at 65 °C extend into the solvent with an increase in pressure and density. Despite this improvement in solvent quality, the solvent conditions remain in the poor solvent regime at all densities examined. For example, in Figure 7, the highest density examined at 65 °C is lower than both ρ_Θ and the UCSD. The poor solvent regime is also consistent with the fitted α values (eq 3) which vary between 0.2 and 0.3 at the highest densities, whereas SCF theory predicts that $\alpha = {}^1/_2$ for infinitely long chains in a Θ solvent.

In Figures 6 and 7, we see similar trends in the chain extension at both 25 and 65 °C for pressures and

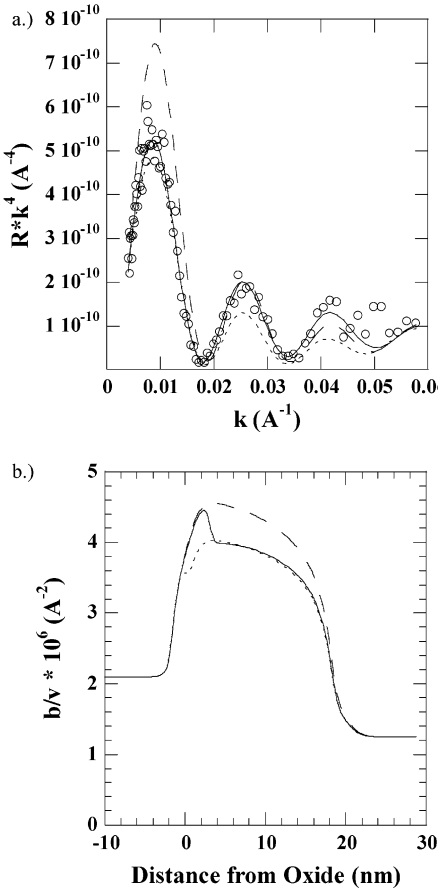

Figure 5. (a) $R*k^4$ vs k. (○) are experimental data at 65 °C and 137.1 atm; (—) is the best-fit. The lines are generated from the respective NSLD profiles in (b). (b) NSLD profiles.

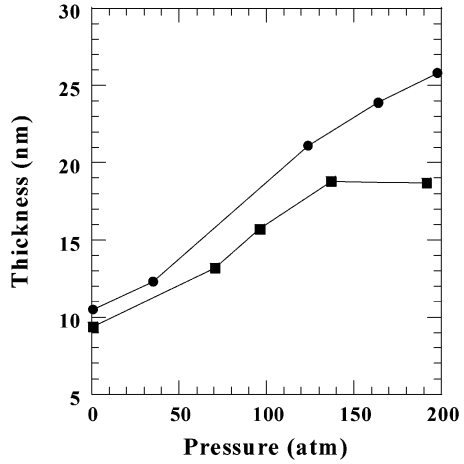

Figure 6. Total *d*-PDMS brush thickness vs CO_2 pressure. (●) are at 25 °C and (■) are at 65 °C.

densities below the UCSD. However, the highest densities examined at 25 °C are above the UCSD and very near ρ_Θ. Interestingly, the thickness of the brush at 25 °C begins to increase more sharply in this high-density region. On the basis of the work of Melnichenko et al.,[15,40] the highest densities examined at 25 °C are near but still below ρ_Θ, and hence the CO_2 is still in the poor-solvent regime. This is also consistent with our fitted α values at 25 °C, which reach a value ~0.4 at the highest densities examined.

Interfacial Structure. An interesting feature in the NSLD profiles is the presence of a distinct region of concentrated polymer near the oxide surface. As seen in Figure 4, the NSLD profiles at the lowest pressures are concentrated in polymer throughout the thickness of the brush due to minimal solvation. When the CO_2 pressure is increased at both temperatures, the outer region of the brush becomes solvated and begins to extend into the CO_2 whereas the brush remains concentrated in polymer near the oxide surface. At the highest pressures, the contrast between the NSLD of the outer solvated region and the concentrated region becomes greater and the regions become more distinguishable. At the lowest pressures, there still appears to be a concentrated region, but the contrast between the concentrated region and the outer region of the brush is much smaller. This smaller contrast is due to the fact that at the lowest pressures the solvent densities are so low that the brush is essentially exposed to a nonsolvent. Therefore, the brush resides in a collapsed state due to insufficient solvation, resulting in a high monomer concentration throughout the thickness of the brush.

Figure 8 shows the breakdown of the total brush thickness into individual components consisting of the thickness of the outer solvated region and the thickness of the inner concentrated region. Interestingly, we see

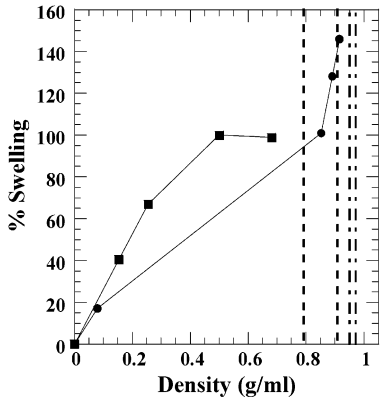

Figure 7. Percent change in brush thickness vs CO_2 density. (●) are at 25 °C and (■) are at 65 °C. From left to right the vertical lines represent the (- - -) UCSD at 65 °C, (- - -) UCSD at 25 °C, (- — -) ρ_Θ at 65 °C, and (- — -) ρ_Θ at 50 °C.

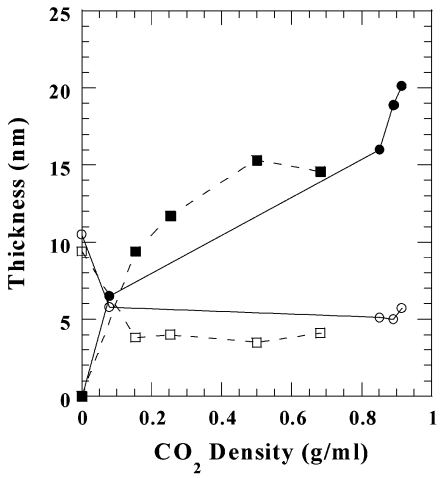

Figure 8. Thickness of solvated and concentrated regions of *d*-PDMS brush vs CO_2 density. (●) represent the outer solvated region of the brush at 25 °C, (○) represent the polymer-concentrated region at 25 °C, (■) represent the solvated region of the brush at 65 °C, and (□) represent the polymer-concentrated region at 65 °C.

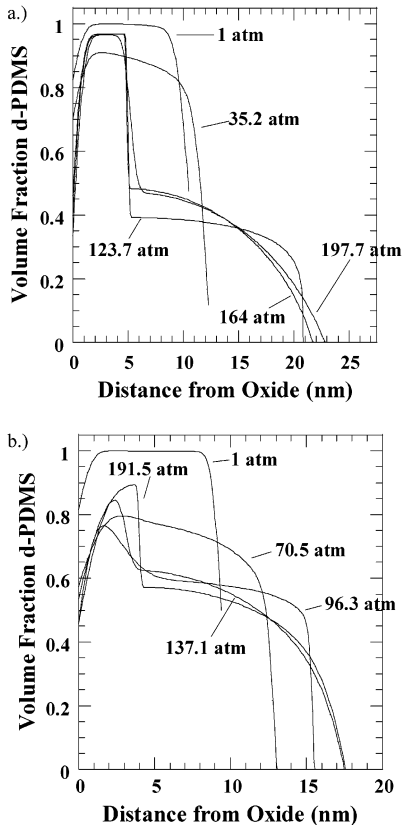

Figure 9. (a) Volume fraction profiles for *d*-PDMS brush at 25 °C. (b) Volume fraction profiles at 65 °C.

that the thickness of the outer solvated region follows the same trend as the total brush thickness, whereas the thickness of the concentrated region initially decreases with increasing density and then becomes relatively constant. Another interesting feature is that the concentrated region at 25 °C is ~25% thicker than at 65 °C.

The NSLD profiles in Figure 4 can be converted readily to volume fraction profiles. In general, the mixture NSLD for a binary *d*-PDMS/CO_2 system is

$$(\mathrm{NLSD})_{\mathrm{mix}}(z) = \phi(z)_{d-\mathrm{PDMS}}(\mathrm{NSLD})_{d-\mathrm{PDMS}} + (1 - \phi(z)_{d-\mathrm{PDMS}})(\mathrm{NSLD})_{\mathrm{CO_2}} \quad (9)$$

where $(\mathrm{NSLD})_{\mathrm{mix}}(z)$ is the mixture NSLD at a distance z from the grafting plane, $(\mathrm{NSLD})_{d-\mathrm{PDMS}}$, and $(\mathrm{NSLD})_{\mathrm{CO_2}}$ are the pure component NSLD's for *d*-PDMS and CO_2, respectively, and $\phi(z)_{d-\mathrm{PDMS}}$ is the volume fraction of *d*-PDMS at a distance z from the grafting plane. Typically, the pure component NSLD value for an incompressible solvent is taken as the NSLD value of the solvent at the temperature where the scan is taken. Our system is more complicated since it is well-known that the molar volume of CO_2 within the polymer can be much different than the molar volume of the bulk CO_2 at the system temperature and pressure. Therefore, the $(\mathrm{NSLD})_{\mathrm{CO_2}}$ at each temperature and pressure is calculated such that the resulting volume fraction profile gives the same grafted amount of polymer (see eq 4) as the solvent-less case. This approach ensures conservation of mass. The volume fraction profiles are shown in Figure 9 for both temperatures.

The volume fraction profiles indicate very concentrated brushes at the lowest CO_2 pressures. As the CO_2 pressure and thus density are increased, the polymer volume fraction profiles for the outer regions of the brush become diluted and take a more parabolic shape at both temperatures. In addition, we observe a region near the substrate that remains concentrated in polymer at all of the pressures. At 25 °C, this concentrated region has a *d*-PDMS volume fraction between 0.90 and 0.95, whereas at 65 °C the concentrated region has a *d*-PDMS volume fraction between 0.78 and 0.90. In addition, a small depletion in the polymer volume fraction is observed very near the substrate at both temperatures. This depletion is likely due to entropic repulsion at the substrate and/or roughness at the polymer/substrate interface. The volume fraction profiles also show that the outer solvated regions of the brushes generally have a lower volume fraction at 25 °C than at 65 °C. This increased dilution is due to the markedly higher CO_2 densities and hence better solvent qualities at 25 °C.

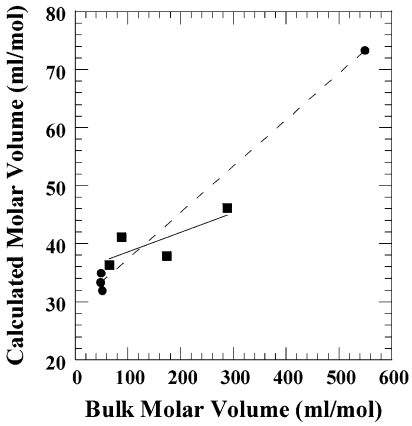

Figure 10. CO_2 molar volume corresponding to the calculated pure component $(\mathrm{NSLD})_{\mathrm{CO_2}}$ used in constructing the volume fraction profiles vs bulk CO_2 molar volume. (●) are at 25 °C and (■) are at 65 °C. The lines highlight the trends in the data.

The CO_2 molar volumes corresponding to the calculated pure component $(\mathrm{NSLD})_{\mathrm{CO_2}}$'s used in constructing the volume fraction profiles are plotted vs the bulk CO_2 molar volume in Figure 10. The CO_2 molar volumes are calculated from the pure component $(\mathrm{NSLD})_{\mathrm{CO_2}}$ by solving eq 2 for $M_{\mathrm{wCO_2}}/\rho_{\mathrm{CO_2}}$. The calculated pure component $(\mathrm{NSLD})_{\mathrm{CO_2}}$'s correspond to liquidlike CO_2 molar volumes even when the bulk CO_2 molar volumes are much larger. The CO_2 contracts as it dissolves in the polymer brush.

Discussion

The lower critical solution temperature (LCST) type phase separation between polymers and supercritical fluid CO_2 is driven by an increase in entropy. Analogously, in a compressible CO_2 solvent, entropy is gained when CO_2 expands away from the grafted chains into the bulk to increase its volume.[33] The driving force for this expansion becomes smaller as the bulk CO_2 density increases, e.g., above the UCSD. Furthermore, the energy of interaction between monomer and CO_2 increases and becomes closer to that between two monomers as the CO_2 density increases. Therefore, at high CO_2 density the *d*-PDMS brush is more solvated, with a lower segment volume fraction in the outer solvated region, and extends further into CO_2. At CO_2 densities below the UCSD, the entropic gains for the CO_2 expansion away from the chains and into the lower density

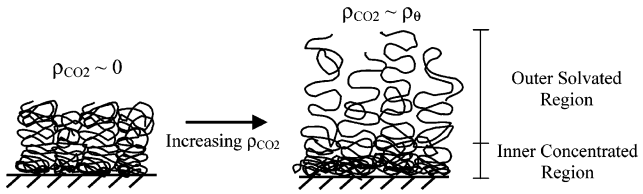

Figure 11. Effect of CO_2 density on chain extension and interfacial structure. A polymer-concentrated region and a solvated region are observed in the brush structure.

bulk solvent become more important, resulting in chain collapse. Here there is insufficient solvation to screen the attractive intra- and interchain interactions.

The *relative* extension at 65 °C is greater than at 25 °C as shown in Figure 7. Attractive dipole−dipole monomer−monomer interactions become less important as temperature is increased at constant density whereas solvation of monomer by CO_2 due to van der Waals interactions is relatively constant. This trend likely explains the increase in the relative chain extension. Similar behavior was observed by Luna-Barcenas et al. using Monte Carlo simulations, where they found that the mean-square end-to-end distance of a single chain in a supercritical fluid also increased when raising temperature at constant density.[51] Temperature effects on the attractive monomer−monomer interactions are also the likely reason for smaller thickness and volume fractions for the polymer-concentrated regions at the higher temperature. In addition, temperature effects on solvent quality have been observed in recent SANS experiments on semidilute bulk PDMS/CO_2 solutions.[15,40] Melnichenko et al. reported that ρ_Θ increased from 0.87 to 0.97 g/mL when the temperature was decreased from 80 to 50 °C.[15,40] Thus, they find that the solvent quality at a given CO_2 density is better for higher temperatures.

We observe two distinct regions in the NSLD and volume fraction profiles for the end-grafted brushes, as shown schematically in Figure 11. First, there exists a polymer-concentrated region near the oxide where the *d*-PDMS volume fraction changes little with pressure from 1 atm to the highest pressure studied near ρ_Θ. CO_2 penetrates this region very little. The second region observed in our profiles is the outer solvated portion of the brush, which is relatively dilute and extends progressively further out into the CO_2 as the solvent quality is improved. Furthermore, the volume fraction profiles in this portion of the brush evolve from step-function profiles at the lowest CO_2 densities to more parabolic profiles at the highest CO_2 densities.

While most studies of chemically end-grafted brushes are done on noninteracting or repulsive substrates, there are a few examples of theoretical,[52] simulation,[22,53] and experimental[23,25] studies that have examined the structure of end-grafted brushes on interacting surfaces. For example, Chakrabarti et al.[53] used Monte Carlo simulations to determine the volume fraction profiles of end-grafted brushes on attractive substrates. They studied the effect of both short-range (contact type) and long-range attractive interactions. For the case of short-range interactions in a good solvent, they found that the monomer density profile decays monotonically in the vicinity of the grafting plane, whereas far away from the wall the profile was parabolic and similar to the nonadsorbing case. For the case of long-range interactions (attractive square-well potential) in a good solvent, Chakrabarti et al. found a concentrated region of polymer with a constant volume fraction throughout the

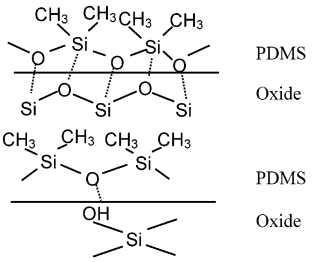

Figure 12. Interaction mechanisms for PDMS with SiO_x surface.

range of the attractive potential. Outside the potential range, the profile had a parabolic decay similar to the nonadsorbing case. Overall, their results show good agreement with SCF calculations.[52,53]

Similar to simulations[53] that include a long-range attraction between the surface and the brush, our results show two distinct regions in the brush volume fraction profiles. Previous molecular dynamics[22] and experimental studies have also observed this behavior.[25] Perahia et al.[25] determined the volume fraction profiles of weakly end-grafted polystyrene brushes on silicon in equilibrium with a solution of unbound polymer. They concluded that away from the grafting surface the brush profile is determined solely by solvation forces, whereas near the grafting surface the interaction of the polymer with the surface strongly influences the profile.[25] Despite the fact that our results also show two distinct regions in brush structure, we will demonstrate some significant differences in the details of our structure and in the relevant intermolecular forces.

For our system, it is known that CO_2 will adsorb onto silica surfaces,[54,55] but it has been reported that CO_2 only weakly interacts with surface silanols.[56] In contrast, it has been demonstrated that PDMS strongly interacts with silica surfaces via mechanisms such as those shown in Figure 12.[46−48,50] There are two key ways that PDMS could interact with SiO_x surfaces. First, from Table 1, there are ∼0.3−0.4 chains/nm^2. A fully hydroxylated SiO_x surface contains ∼4.6 silanols/nm^2.[57] Thus, *d*-PDMS is only bonded to ∼7−8% of the available silanol groups, leaving many unreacted silanols to form hydrogen bonds with the oxygen groups in the *d*-PDMS backbone. Second, long-range Hamaker interactions between the substrate and the brush also attract the *d*-PDMS chains to the SiO_x surface.

To study the long-range van der Waals interaction, the Hamaker constant (using Lifshitz theory)[58] was calculated for a PDMS sphere, with a radius corresponding to the area/chain (see Table 1), interacting with a silica surface. The van der Waals interaction energy remains on the order of $\sim kT$ and has a substantial influence at distances of 3−4 nm away from the substrate. Thus, the interfacial structure observed for the *d*-PDMS brushes is governed by several different interactions including strong hydrogen bonding with surface silanols, long-range van der Waals attractive interactions with the substrate, attractive intra- and interchain interactions, and solvation of the chains by CO_2.

As seen for previous studies in incompressible solvents,[22,25,53] the solvated region of our brush becomes more parabolic with improved solvent quality. Despite this similarity, major differences are evident. In our system, the solvent quality is varied over an enormous range from an ideal gas (nonsolvent) to a near-Θ

solvent. At the lowest pressures, the brush is in a concentrated, fully collapsed state. As the CO_2 pressure is initially increased, the concentrated region shrinks markedly as CO_2 pulls segments into the outer solvated region. In contrast, the thickness of the concentrated region changes very little with temperature in the previous studies in incompressible solvents.

The volume fraction and thickness of our outer solvated region also change much more with solvent quality than for the previous studies. In previous studies involving incompressible UCST-type solvents, it is observed that the brush profiles are only weakly dependent on temperature in the poor-solvent regime while remaining significantly swollen with solvent relative to the fully collapsed state.[23,29] The greater variation for our compressible system results from the ability to change pressure and temperature, independently, and the larger adjustability of the solvent quality. In essence, the solvent quality becomes much poorer for CO_2 than for these liquid solvents, leading to greater collapse. The balance of the effects of the various interactions on the brush structure changes much more dramatically due to the enormous change in solvent quality, the presence of profound density differences between the chain region and the surrounding solvent, the presence of an LCST instead of an UCST, and a strong long-ranged Hamaker interaction from the surface. The LCST is manifested by the large volume expansion from the region in the chains to the outer bulk solvent. The long-range Hamaker interaction attracts polymer chains from low-density regions away from the substrate to higher density regions toward the substrate. Thus, the chains do not remain as swollen with solvent as in the case of the studies in incompressible solvents. This ability to perturb the structure is magnified by the large compressibility and free volume for our system and by the high asymmetry in the segment−substrate, segment−segment, and segment−CO_2 interactions. The high asymmetry arises from the unusually low polarizability per volume for CO_2, that is, its weak solvent strength and van der Waals forces relative to PDMS. At much higher CO_2 densities, beyond our experimental limit, this asymmetry will be reduced, the compressibility will be lower, and the brush profile may be expected to become closer to that observed in incompressible solvents.

Experimental measurements of the structure of end-grafted brushes in highly compressible solvents have not been reported previously. However, Monte Carlo simulations and LFSCF theory have been used to explore the structure and interactions of end-grafted polymers in supercritical fluids.[32−34] Qualitatively, the behavior of the chain extension in this study, as a function of solvent density, is in rough agreement with theory and simulation. In contrast, whereas the shapes of the profiles change markedly with density in Figure 9, they change little in the simulations over the range of bulk solvent densities studied. Simulations generally found that the segment density profiles were parabolic with an exponential tail, even at densities in the poor-solvent regime.[34] These differences in the chain distributions are likely due to the shorter chains, use of a noninteracting surface, and the smaller σ^* values used in the simulations.

The understanding of brush conformation in this study provides insight into colloid flocculation in compressible solvents. Many previous studies of the polymeric stabilization of colloidal dispersions in conventional liquid solvents have suggested that colloids will flocculate at the Θ temperature.[16] In supercritical fluids, the relationship between the density where flocculation occurs, the critical flocculation density (CFD), and the ρ_Θ is somewhat uncertain. For example, various simulation and theoretical studies in supercritical fluids predict that surfaces and colloids with adsorbed and grafted stabilizers will flocculate at the UCSD for the bulk stabilizer/solvent system.[33,59] The UCSD is the critical density for finite molecular weight polymer corresponding to the entropically driven LCST. These studies focused on symmetric systems where a segment on the polymer chain was equivalent to a solvent molecule. This prediction is in agreement with experiment for emulsions stabilized with PFOA.[35] PFOA has a low cohesive energy density, making it fairly symmetric with CO_2. Other studies with grafted PDMS stabilizers were unable to achieve stable dispersions at solvent densities well above the UCSD but below ρ_Θ.[39] The higher cohesive energy density for PDMS makes it less symmetric with CO_2, complicating the physics.

The present study of the structure of the *d*-PDMS/silicon substrate sheds light into the density effect on colloid stability. As expected, the *d*-PDMS brushes extend further into the solvent with increased CO_2 pressures and thus densities at both temperatures, as solvent quality is a strong function of density.[32] Furthermore, at 25 °C the chain extension increases sharply in the vicinity of the UCSD and ρ_Θ. Therefore, better stabilization may be expected well above the UCSD. Consequently, it may be expected that the above PDMS-grafted silica colloids would have become stable at densities approaching ρ_Θ (well above the limitation of the experimental apparatus).[39] The PDMS system is not as symmetric with CO_2 as PFOA.[6] Therefore, simulation should be performed in the future on asymmetric systems to relate the CFD to ρ_Θ.

The brush profiles indicate that the ability of CO_2 to pull the chains into the outer solvated regions is somewhat limited relative to the earlier studies in incompressible solvents. The presence of an attractive surface reduces the *d*-PDMS brush thickness, at a given CO_2 solvent quality, relative to a noninteracting surface.[53] This attraction is one reason that PDMS chains do not provide steric stabilization for silica colloids even in cases above the UCSD where, in the absence of a surface, the chains are soluble in CO_2.

Conclusions

High-pressure neutron reflectivity was used to measure the chain extension and segment density profiles of end-grafted *d*-PDMS brushes exposed to liquid and supercritical CO_2. The solvent quality was tuned continuously over an enormous range from ideal gas conditions to a near-Θ solvent by varying temperature and CO_2 density. At 25 °C, the chain extension increases sharply as the CO_2 density is increased above the UCSD to densities near ρ_Θ.

Two distinct regions are observed in the brush structures. An inner concentrated region of *d*-PDMS is observed near the grafting surface due to attractive intra- and interchain interactions, hydrogen bonding between *d*-PDMS and surface silanols, and long-range attractive van der Waals interactions between the *d*-PDMS and the SiO_x substrate. In contrast, the outer region of the brush becomes solvated and extends as

the CO_2 density is increased. The volume fraction profiles for the solvated region evolve from block profiles to more parabolic profiles as the solvent quality is improved. The thickness and volume fraction profiles for the brushes change much more with solvent quality than for previous studies in incompressible solvents. This greater variation arises from the large adjustability of the solvent quality due to the compressible nature of the solvent, large density (free volume) differences between the brush region and the solvent, the presence of an LCST instead of an UCST, the high asymmetry in the segment−substrate, segment−segment, and segment−CO_2 interactions, and the effect of this asymmetry on the long-ranged interactions between the substrate and the compressible solvent. The unusually large width of the inner concentrated brush region where solvation is minimal limits the chain extension and may explain limitations in steric stabilization observed for silica colloids in CO_2 with PDMS stabilizers at solvent densities above the UCSD.

Acknowledgment. This work was supported by the by the STC program of the NSF under agreement CHE-9876674, the Welch Foundation, the Department of Energy, and the National Science Foundation (DMR0072809). The authors acknowledge Dr. John Webster, Kristopher Lavery, and Timothy Francis for their help with the NR experiments.

Supporting Information Available: Summary table of bulk *d*-PDMS and CO_2 NSLD values and of fitted α values. This material is available free of charge via the Internet at http://pubs.acs.org.

References and Notes

(1) Taylor, D. K.; Carbonell, R.; DeSimone, J. M. *Annu. Rev. Energy Environ.* **2000**, *25*, 115−146.
(2) Lee, C. T.; Psathas, P. A.; Johnston, K. P.; deGrazia, J.; Randolph, T. W. *Langmuir* **1999**, *15*, 6781−6791.
(3) Lee, C. T.; Psathas, P. A.; Ziegler, K. J.; Johnston, K. P.; Dai, H. J.; Cochran, H. D.; Melnichenko, Y. B.; Wignall, G. D. *J. Phys. Chem. B* **2000**, *104*, 11094−11102.
(4) Canelas, D. A.; Betts, D. E.; DeSimone, J. M.; Yates, M. Z.; Johnston, K. P. *Macromolecules* **1998**, *31*, 6794−6805.
(5) Calvo, L.; Holmes, J. D.; Yates, M. Z.; Johnston, K. P. *J. Supercrit. Fluids* **2000**, *16*, 247−260.
(6) O'Neill, M. L.; Cao, Q.; Fang, R.; Johnston, K. P.; Wilkinson, S. P.; Smith, C. D.; Kerschner, J. L.; Jureller, S. H. *Ind. Eng. Chem. Res.* **1998**, *37*, 3067−3079.
(7) Sarbu, T.; Styranec, T.; Beckman, E. J. *Nature (London)* **2000**, *405*, 165−168.
(8) Sarbu, T.; Styranec, T. J.; Beckman, E. J. *Ind. Eng. Chem. Res.* **2000**, *39*, 4678−4683.
(9) Drohmann, C.; Beckman, E. J. *J. Supercrit. Fluids* **2002**, *22*, 103−110.
(10) Mawson, S.; Yates, M. Z.; O'Neill, M. L.; Johnston, K. P. *Langmuir* **1997**, *13*, 1519−1528.
(11) Raveendran, P.; Wallen, S. L. *J. Am. Chem. Soc.* **2002**, *124*, 7274−7275.
(12) Johnston, K. P.; Cho, D.; DaRocha, S. R. P.; Psathas, P. A.; Ryoo, W.; Webber, S. E.; Eastoe, J.; Dupont, A.; Steytler, D. C. *Langmuir* **2001**, *17*, 7191−7193.
(13) McClain, J. B.; Londono, D.; Combes, J. R.; Romack, T. J.; Canelas, D. A.; Betts, D. E.; Wignall, G. D.; Samulski, E. T.; DeSimone, J. M. *J. Am. Chem. Soc.* **1996**, *118*, 917−918.
(14) Chillura-Martino, D.; Triolo, R.; McClain, J. B.; Combes, J. R.; Betts, D. E.; Canelas, D. A.; DeSimone, J. M.; Samulski, E. T.; Cochran, H. D.; Londono, J. D.; Wignall, G. D. *J. Mol. Struct.* **1996**, *383*, 3−10.
(15) Melnichenko, Y. B.; Kiran, E.; Wignall, G. D.; Heath, K. D.; Salaniwal, S.; Cochran, H. D.; Stamm, M. *Macromolecules* **1999**, *32*, 5344−5347.
(16) Napper, D. H. *Polymeric Stabilization of Colloidal Dispersions*; Academic Press: London, 1983.
(17) Milner, S. T. *Science* **1991**, *251*, 905−914.
(18) de Gennes, P. G. *Macromolecules* **1980**, *13*, 1069−1075.
(19) Zhulina, E. B.; Borisov, O. V.; Pryamitsyn, V. A.; Birshtein, T. M. *Macromolecules* **1991**, *24*, 140−149.
(20) Milner, S. T.; Witten, T. A.; Cates, M. E. *Macromolecules* **1988**, *21*, 2610−2619.
(21) Lai, P.; Binder, K. *J. Chem. Phys.* **1992**, *97*, 586−595.
(22) Grest, G. S.; Murat, M. *Macromolecules* **1993**, *26*, 3108−3117.
(23) Karim, A.; Satija, S. K.; Douglas, J. F.; Ankner, J. F.; Fetters, L. J. *Phys. Rev. Lett.* **1994**, *73*, 3407−3410.
(24) Kent, M. S.; Lee, L. T.; Factor, B. J.; Rondelez, F.; Smith, G. S. *J. Chem. Phys.* **1995**, *103*, 2320−2342.
(25) Perahia, D.; Wiesler, D. G.; Satija, S. K.; Fetters, L. J.; Sinha, S. K.; Milner, S. T. *Phys. Rev. Lett.* **1994**, *72*, 100−103.
(26) Habicht, J.; Schmidt, M.; Ruhe, J.; Johannsmann, D. *Langmuir* **1999**, *15*, 2460−2465.
(27) Auroy, P.; Auvray, L.; Leger, L. *Macromolecules* **1991**, *24*, 2523−2528.
(28) Kent, M. S.; Majewski, J.; Smith, G. S.; Lee, L. T.; Satija, S. *J. Chem. Phys.* **1998**, *108*, 5635−5645.
(29) Kent, M. S.; Majewski, J.; Smith, G. S.; Lee, L. T.; Satija, S. K. *J. Chem. Phys.* **1999**, *110*, 3553−3565.
(30) Russell, T. P. *Mater. Sci. Rep.* **1990**, *5*, 171−271.
(31) Penfold, J. *Curr. Opin. Colloid Interface Sci.* **2002**, *7*, 139−147.
(32) Peck, D. G.; Johnston, K. P. *Macromolecules* **1993**, *26*, 1537−1545.
(33) Meredith, J. C.; Johnston, K. P. *Macromolecules* **1998**, *31*, 5518−5528.
(34) Meredith, J. C.; Sanchez, I. C.; Johnston, K. P.; Pablo, J. J. *J. Chem. Phys.* **1998**, *109*, 6424−6434.
(35) O'Neill, M. L.; Yates, M. Z.; Harrison, K. L.; Johnston, K. P.; Canelas, D. A.; Betts, D. E.; DeSimone, J. M.; Wilkinson, S. P. *Macromolecules* **1997**, *30*, 5050−5059.
(36) Liu, L.; Cheng, Z.; Inomata, K.; Zhou, S.; Chu, B. *Macromolecules* **1999**, *32*, 5836−5845.
(37) Taylor, D. K.; Keiper, J. S.; DeSimone, J. M. *Ind. Eng. Chem. Res.* **2002**, *41*, 4451−4459.
(38) McClain, J. B.; Betts, D. E.; Canelas, D. A.; Samulski, E. T.; DeSimone, J. M.; Londono, J. D.; Cochran, H. D.; Wignall, G. D.; Chillura-Martino, D.; Triolo, R. *Science* **1996**, *274*, 2049−2052.
(39) Yates, M. Z.; Shah, P.; Johnston, K. P.; Lim, K. T.; Webber, S. *J. Colloid Interface Sci.* **2000**, *227*, 176−184.
(40) Melnichenko, Y. B.; Kiran, E.; Heath, K. D.; Salaniwal, S.; Cochran, H. D.; Stamm, M.; Van Hook, W. A.; Wignall, G. D. *J. Appl. Crystallogr.* **2000**, *33*, 682−685.
(41) Cras, J. J.; Rowe-Taitt, C. A.; Nivens, D. A.; Ligler, F. S. *Biosens. Bioelectron.* **1999**, *14*, 683−688.
(42) RamanchandraRao, V. S.; Gupta, R. R.; Russell, T. P.; Watkins, J. J. *Polym. Mater. Sci. Eng.* **2001**, *84*, 204−205.
(43) Gupta, R. R.; Lavery, K. A.; Francis, T. J.; Webster, J. R. P.; Smith, G. S.; Russell, T. P.; Watkins, J. J. *Macromolecules* **2003**, *36*, 346−352.
(44) Sears, V. F. *Neutron News* **1992**, *3*, 26−37.
(45) Zeghal, M.; Deloche, B.; Albouy, P. A.; Auroy, P. *Phys. Rev. E: Stat. Phys., Plasmas, Fluids* **1997**, *56*, 5603−5614.
(46) Perkel, R.; Ullman, R. *J. Polym. Sci.* **1961**, *54*, 127−148.
(47) Ashmead, B. V.; Owen, M. J. *J. Polym. Sci., Part A-2* **1971**, *9*, 331−343.
(48) Patel, A.; Cosgrove, T.; Semlyen, J. A. *Polymer* **1991**, *32*, 1313−1317.
(49) Cosgrove, T.; Turner, M. J.; Thomas, D. R. *Polymer* **1997**, *38*, 3885−3892.
(50) Auvray, L.; Cruz, M.; Auroy, P. *J. Phys. II* **1992**, *2*, 1133−1140.
(51) Luna-Barcenas, G.; Meredith, J. C.; Sanchez, I. C.; Johnston, K. P.; Gromov, D. G.; de Pablo, J. J. *J. Chem. Phys.* **1997**, *107*, 10782−10792.
(52) Marko, J. F.; Johner, A.; Marques, C. M. *J. Chem. Phys.* **1993**, *99*, 8142−8153.
(53) Chakrabarti, A.; Nelson, P.; Toral, R. *Phys. Rev. A: At. Mol. Opt. Phys.* **1992**, *46*, 4930−4934.
(54) Sirard, S. M.; Ziegler, K. J.; Sanchez, I. C.; Green, P. F.; Johnston, K. P. *Macromolecules* **2002**, *35*, 1928−1935.
(55) Strubinger, J. R.; Song, H.; Parcher, J. F. *Anal. Chem.* **1991**, *63*, 98−103.
(56) Tripp, C. P.; Combes, J. R. *Langmuir* **1998**, *14*, 7348−7352.
(57) Iler, R. K. *The Chemistry of Silica*; John Wiley & Sons: New York, 1979.
(58) Israelachvili, J. N. *Intermolecular and Surface Forces*, 2nd ed.; Academic Press: San Diego, CA, 1992.
(59) Meredith, J. C.; Johnston, K. P. In *Supercritical Fluids*; Kiran, E., Debenedetti, P. G., Peters, C. J., Eds.; Kluwer Academic Publishers: Dordrecht, 2000; Vol. 366, pp 211−227.

MA025801W